Rock temperature prior to failure: analysis of 209 rockfall events in the Mont Blanc massif (Western European Alps)

A Legay, Florence Magnin, Ludovic Ravanel

Rock temperature prior to failure: analysis of 209 rockfall events in the Mont Blanc massif (Western European Alps)

A. Legay[1], F. Magnin[1], L. Ravanel[1]

[1] EDYTEM Lab, Université Savoie Mont Blanc, CNRS, Le Bourget-du-Lac, France

Corresponding author: Florence Magnin [florence.magnin@univ-smb.fr]

Key words: rockfall, alpine rockwall, thermal modeling, permafrost, Mont Blanc massif

ABSTRACT

Periglacial rockwalls are affected by an increase in rockfall activity attributed to permafrost degradation. While recent laboratory testing has asserted the role of permafrost in bedrock stability, linking experimental findings to field applications is hindered by the difficulty to assess bedrock temperature at observed rockfall locations and time. In this study, we simulated bedrock temperature for 209 rockfalls inventoried in the Mont Blanc massif between 2007 and 2015 and 209 000 random events artificially created at observed rockfall locations. Real and random events are then compared in a statistical analysis to determine the results significance. Permafrost conditions (or very close to 0 °C) were consistently found for all events with failure depth > 6 m, and for some events affecting depths from 3 to 6 m. Shallower events were likely not related to

permafrost processes. Surface temperatures were significantly high up to at least 2 months prior to failure with the highest peaks in significance 1.5 to 2 months and 1 to 5 days before rockfalls. Similarly, temperature significances at scar depths were significantly high, but steadily decreasing, 1 day to 3 weeks before failure. The study confirms that warm permafrost areas (> -2 °C) are particularly prone to rockfalls, and that failures are a direct response to extraordinary high bedrock temperature in both frozen and unfrozen conditions. The results are promising for the development of a rockfall susceptibility index but uncertainty analysis encourages to use a greater rockfall sample and a different sample of random events.

1. Introduction

Rockwalls can be affected by significant gravity-related transfers of material throughout rockfall, defined here as the detachment of a mass of rock with a volume exceeding 100 m^3 from a series of discontinuities, and its transportation downslope on variable distance[1]. Rockfall is one of the most hazardous geomorphological processes in Alpine massifs and can threaten mountain infrastructure[2–5], tourism[6,7] and valley floors in case of major events[8–12]. Periglacial rockwalls have been increasingly affected by rockfalls[13–18], notably during summer heatwaves[19,20] and permafrost degradation is thus thought to be one of the main factors responsible for these increasing bedrock destabilizations[21–25]. With the projected degradation of alpine permafrost[26], these hazards will likely become a major threat for mountain communities and a better understanding of the thermal context leading to periglacial rockwall failure is therefore crucial.

Laboratory experiments conducted over the past two decades have extensively contributed to understand how thawing bedrock may become unstable. In a first stage, Davies et al.[27] have

demonstrated that besides the normal stress, the strength of an ice filled rock joint is a function of its temperature. It decreases with warming and reaches a minimal value at -0.5 °C. Then, Mamot et al.[28] have refined this analysis showing a decrease of ice-filled joint resistance by a range of 64 - 78 % when the bedrock warms from -10 to -0.5 °C. Those studies agree with former investigations combining field observations and heat conduction modeling to explain the link between the thawing front propagation and boulder fall in periglacial rockwalls[29]. However, Krautblatter et al.[24] have lately explained that the rupture of ice filled joints may only occur at depth < 20 m while, deeper, warming provokes slow deformation along rock-rock contact, meaning that the rupture of ice-filled joints may only explain relatively shallow events. In addition, laboratory experiments have also pointed out that ice-filled joint alteration may also result of enhanced erosion provoked by water percolation and related advective heat transfer[30]. This is supported by field investigations at rockwall sites showing thawing corridors through geophysical soundings[31] or sudden temperature increase in borehole[32]. Water infiltration and circulation may also cause hydrostatic pressure in ice-sealed fractures that could contribute to rockfall triggering[24,25,33,34] as suggested by observations of water together with massive ice in rockfall scars[20–22]. However, determining the role of hydraulic processes in alpine rockfall triggering is challenging because of the lack of fully coupled thermo-hydro-mechanical numerical models and data for parameterization[33].

Despite these limits, the link between rock slope failures and permafrost conditions was confirmed for various events using transient heat conduction models for specific rockfalls[21,22] or through comparison of permafrost map[35] and rockfall inventory[26]. Statistical analysis of climate variables or rock surface temperature evolution also showed a strong link between air temperature anomaly and rockfall occurrence in high mountain[36–38,] while various studies explain that strong thermal

oscillations and related cyclic thermal stress or thermal expansion related to heating may cause rockfall in non-periglacial environments[39–41].

Despite these advances, observations are generally too sparse or inhomogeneous to draw robust statistical analysis of thermal conditions at depth of bedrock failure, which limits the understanding of the link between rockfall and rockwall thermal dynamics and therefore our capacity to predict rockfalls.

Our study proposes to investigate bedrock thermal dynamics prior to rockfall occurrence for 209 inventoried events during the period 2007-2015 in the Mont Blanc massif. It uses a 1D transient thermal model[42] simulating temperature-depth profiles at a daily time step. Absolute temperatures simulated at the rock surface and at the depths of rockfall scars prior to failures are presented but the main part of the analysis is based on a statistical approach in order to minimize biases in results interpretation. Our study addresses the following research questions:

- Which bedrock temperature conditions or dynamics are the most prone to rockfall occurrence?
- Is bedrock temperature experiencing exceptionally high value prior to failure?
- Is there a statistical relationship between bedrock temperature and rock slope destabilization?

The study aims at verifying the hypotheses that the observed rockfalls are a direct reaction to the intense and exceptional summer heatwaves that occurred over the past summers[43–45], and that thawing permafrost (close to 0 °C) areas are the most prone to rockfalls. In this way, it intends to better define the time-lag between the air temperature signal and the bedrock failure and to explore a possible statistical relationship between air temperature, rock temperature dynamics and failure occurrences that would help to predict such events with weather forecast.

2. Study area and rockfall database

The Mont Blanc massif (MBM; Fig. 1), with its highest point at 4809 m a.s.l., is a crystalline massif that extends over an area of 550 km^2 in the Western Alps. It presents two main lithological units: a Variscan metamorphic series in the W and SW of the massif, and an intrusive late-Variscan granite in the central and eastern parts, crosscut by three main sets of shear zones and faults[47]. 27 % of the massif was covered by glaciers in the 2000s[48], and 7-12 % of the MBM area are permafrost-affected rockwalls[49]. Permafrost is largely present above 2600 and 3200 m a.s.l. on north- and south-facing slopes, respectively[49].

In the MBM, infrastructures (cable cars, mountain huts, rack railways[3]) and mountaineers[7] are exposed to rockfall. Rockfalls are surveyed since 2007 by a network of observers[50] focused on the central part (57 %) of the MBM. First based on the use of reporting sheets, the transmission of information is now done more directly (oral communication, telephone, mail) or by using an app. The network of observers is reactivated annually (through articles, meetings, forums, mailing-lists) while amateur climbers are also solicited through posters installed in huts or articles in the specialized press and forums. During each fall, extensive fieldwork is routinely carried out to verify the observations from the network and/or to complete them with further data. In little-visited areas of the mountain range, fieldwork is carried out at locations that were not reported by the network, but identified by correlative deposits. Finally, for each event, the date of occurrence (or observation of the deposit), the precise location of the scar, topographic parameters of the destabilized area (altitude, orientation, slope), the fallen volume, and an estimate of the depth of detachment are documented.

Among all the events inventoried between 2007 and 2015, we selected the 209 rockfalls with all required input data for modeling: coordinates, scar depth, date of failure and MARST (Mean

Annual Rock Surface Temperature). The MARST was extracted at rockfall locations from the 4-m-resolution map created by Magnin et al.[35]. This map is based on a statistical model calibrated by Boeckli et al.[51] using MARST measurements from the European Alps, computed potential incoming solar radiation and modeled air temperature.

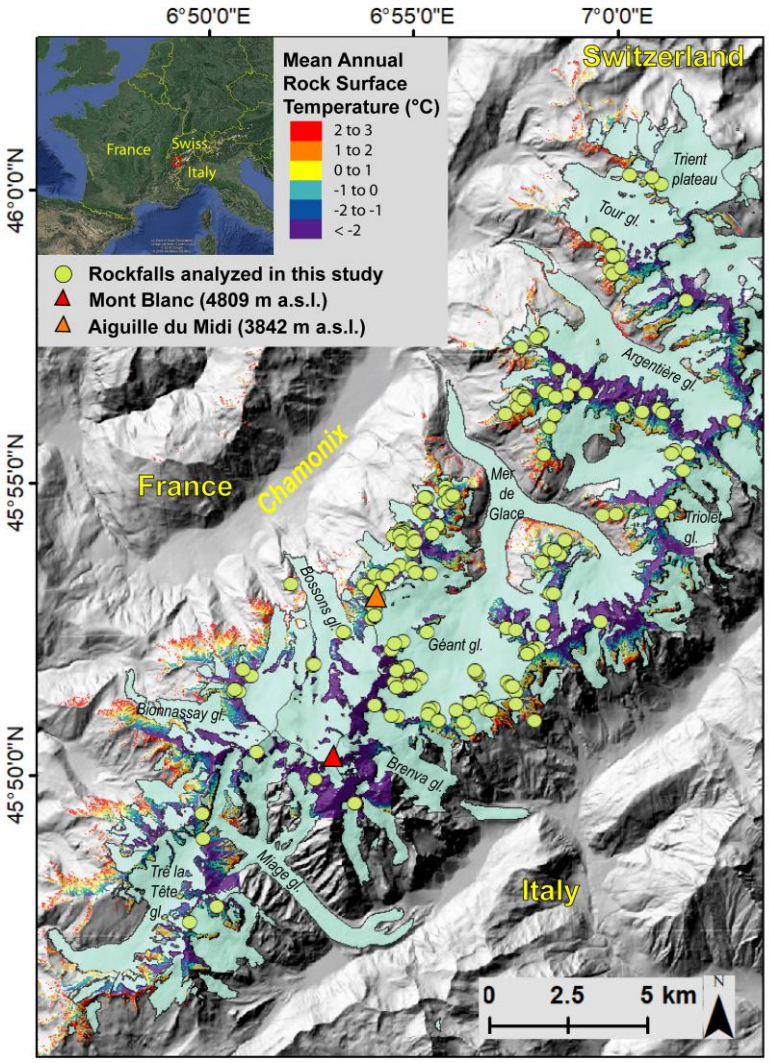

Figure 1. The Mont Blanc massif, the MARST distribution and the location of rockfalls analyzed in this study.

Summary characteristics of this rockfall database are displayed in Table 1 and their distribution displayed in Figure 1. The detailed characteristics are provided in Table S1. About 5% of the rockfalls (10 events) have a MARST > 2 °C, meaning that they are likely in non-permafrost conditions. Indeed, according to Hasler et al.[52], permafrost might be found below MARST up to 3 °C due to the cooling effect of shallow snow cover and air ventilation into fractures. But since the MARST map is built upon mean air temperature for the period 1961-1990 which was about 1 °C cooler than the recent period[35], we assume that permafrost may exist below MARST up to 2 °C. In addition, 23 events (11%) have MARST between 0 and 2 °C and are thus likely in discontinuous and/or warm permafrost conditions.

3. Methods

The goal of our research was to model a temperature-depth (T_z) profile at rockfall locations in order to assess the thermal conditions prior to failure. The simulations were conducted in 1D and intended to represent bedrock temperature perpendicular to the rock surface (Fig. 2). In steep alpine rockwalls, temperature at depth is partly driven by lateral heat fluxes induced by the topographical settings which provoke high surface temperature variability[53]. Thus, we developed an algorithm which accounts for possible lateral heat fluxes in order to correct the modeled T_z profile. In this section, we introduce the so-called CryoGRID2 model (sect. 3.1) that we used to simulate heat transfer, the forcing data and bottom heat flux correction algorithm (sect. 3.2), the model fitting approach (sect. 3.3), the uncertainty calculations (sect. 3.4), and the model implementation at each rockfall location (sect. 3.5).

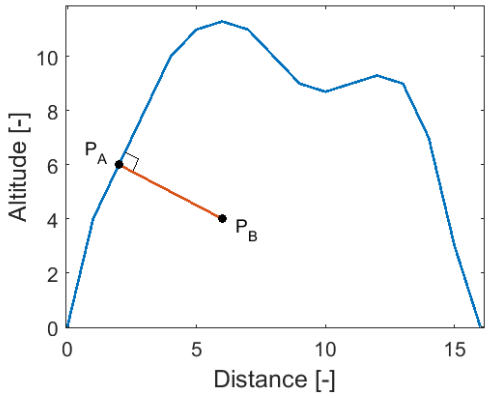

Figure 2. Simplified sketch illustrating the modeled T_z profiles. The blue line represents a topographical profile. P_A is the surface point where the rockfall occurred. P_B is the bottom point of the profile. The red line is the profile where the temperature was calculated at chosen spatial and temporal steps. Altitude and distance are in arbitrary units.

3.1. Heat diffusion modeling with CryoGRID2

We used CryoGRID2 for simulating T_z profiles, a MATLAB diffusive transient thermal 1D model developed by Westermann et al.[42] solving a nonlinear diffusion equation over time. Initially developed for permafrost issues, it solves the conductive heat transfer by taking into account rock properties, air content, water/ice content, and related thawing/freezing processes through latent heat consumption and release. The top of the profile was forced by a surface temperature time series (Dirichlet condition). At the bottom, the profile was forced by a thermal flux (Neumann condition). At every time step, the profile at time n-1 was used as an input for calculating spatial derivatives. At the first time step, we derived an initialization profile by taking the steady state approximation of the equation with the mean of the surface temperature time series for the Dirichlet condition and the first thermal flux for the Neumann condition. This first thermal flux is derived by assuming that the temperature of the profile bottom is equal to the mean of the surface temperature time series (sect. 3.2). CryoGRID2 can handle snowpack at the rock surface. However, since it is almost impossible to construct or obtain such data in steep alpine rockwalls

where snow depth is highly variable, snow was neglected in the present study. A summary of the CryoGRID2 principal input parameters and outputs are available in Supplements (Table S2).

3.2. Forcing data and correction heat flux

The top of the T_z profiles was forced with Rock Surface Temperature (RST) time series derived from the summation of an air temperature anomaly to the MARST extracted at rockfall locations (sect. 2). The air temperature anomaly was calculated in comparison to the 1961-1990 mean air temperature used to derive the MARST map (sect. 2) and from the daily air temperature recorded by *Météo France* at Chamonix (1042 m a.s.l.) since 1993 (beginning of hourly air temperature records), similarly to Magnin et al.[26].

We created a correction flux applied at the profile bottom (Neumann condition) to account for possible lateral heat fluxes coming from surrounding rock faces by using the MARST map (Fig. 1), the 4-m-resolution DEM used to map the MARST and the Chamonix air temperature anomaly time series. We first searched for all surrounding rock faces that may influence the heat fluxes at P_B (see Fig. 2 for P_B) as detailed in the Supplement S1 to obtained N points $(P_i)_{i \in [1:N]}$ at similar altitude than P_A and which were assumed to influence the lower part of the modeled T_z profile (Fig. 3).

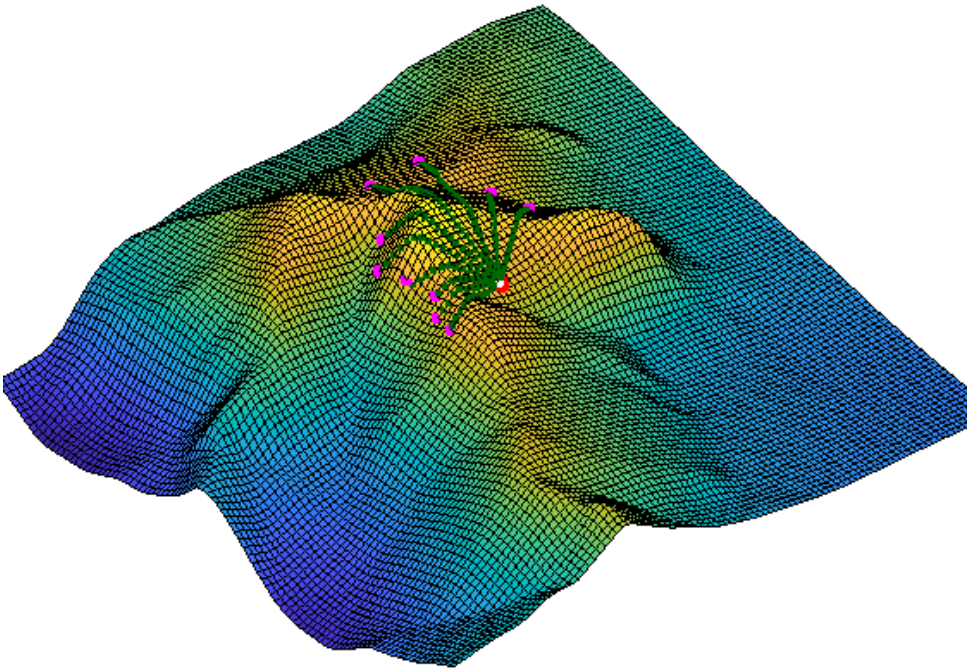

Figure 3. Illustration of the searching method. The 4-m-resolution DEM is represented on a 200 × 200 m square that contains a 200 m radius circle research limit. The white dot in the center is the surface point P_A (see Fig. 2 for P_A) which is the top of the T_z profile. The red dots surrounding P_A represent all the directions eliminated at the first r-step (see Supplement S1). The green dots represent the research directions. Finally, the magenta dots are the selected points for the correction heat flux calculation. Units and the scale are intentionally hidden to lighten the figure. Likewise, only 20 different directions are plotted (instead of 100 used in this study) to help the readability.

We then applied thermal fluxes coming from the selected points. For every point P_i, the MARST at P_i location ($MARST_i$) is extracted from the map and distance d_i between P_i and the bottom point P_B of the modeled T_z profile was calculated. For calculating the i^{th} flux, we separated two cases according to d_i (> or < to 30 m) as detailed in the Supplement S1.

We thus determined the thermal flux $j_{Q,i}(t)$ of all P_i and calculated the global $j_Q(t)$ as follows:

$$j_Q(t) = c_{exp} \frac{\sum_{i=1}^{N} j_{Q,i}(t)}{100} \qquad (1)$$

We divided by 100 because we explored 100 directions, the final flux being an equivalent of a discrete integral. All the fluxes had different directions and different application surfaces. However, we applied all of them at P_B. For considering that, we corrected the final flux by an experimental coefficient c_{exp}. This coefficient was fitted at the same time as the other model parameters (sect. 3.3).

3.3. Model fitting

The simulated transient temperature fields are affected by a set of parameters related to bedrock properties and model characteristics (Table S2). Principal parameters are listed below and have been fitted by running a host of test values until a minimal difference between simulated and measured temperature profiles into boreholes was achieved.

- The rock thermal conductivity ($k_{bedrock}$), the rock volumetric heat capacity ($c_{bedrock}$), the porosity (φ) and the total water content ($\theta_{w,tot}$), which can be assimilated to the bedrock saturation, all change the soil thermal diffusivity, *i.e.* the time needed for the rock to reach thermal equilibrium.
- Van Genuchten parameters (S2) θ_r, α and n change the (θ_{sat},T) curve. The exact influence is not detailed here but, for example, a higher α will impact the dynamics by requiring a higher temperature for melting all the ice.
- c_{exp} changes the magnitude of the lateral heat fluxes (sect. 3.2). For example, the higher is c_{exp}, the stronger is the cooling effect of opposite north faces on south faces and *vice versa.*
- Spin-up parameters change the accuracy of the results during the first years of simulation. Tests we performed showed that three years of spin-up are enough for limiting errors under 0.1 °C the first year of simulation and that this error quickly decreases over time.

Borehole temperature measurements used for model fitting were collected at the Aiguille du Midi[15] (ADM; 3852 m a.s.l.; Fig. 1). Three 10-m-deep boreholes have been drilled in 2009 in SE, NE and NW-exposed rock faces with varying slope conditions (55 ° to sub-vertical) and snow deposits (from continuous and rather thick to discontinuous and thin snow cover, or very local snow deposit). The NE and NW exposed boreholes (respectively BH_E and BH_N) have been equipped with 15 thermistor-chains spread between 0.3 and 10 m depth, while the SE exposed borehole (BH_S) has 14 sensors spread between 0.14 nd 9.64 m depth. They have been recording temperature since December 2009 (except BH_E: April 2010) at a 3-hour time interval. Model fitting was performed at a daily time step using temperature time series at the shallowest depths as forcing temperature time series at the top of the model domain. The simulated T_z profiles were then compared with measured temperatures in the boreholes.

Minimization of the Root Mean Square Error (RMSE) between simulations and boreholes time series were obtained with parameter values displayed in Table 2. Figure 4a displays a simulated T_z profile for a 9 years period with the best-fitted bedrock properties while Figure 4b displays the difference between the measured and the modeled temperature (interpolated between sensors).

Figure 5 presents the error distribution obtained with the parameters displayed in Table 2. All the normality tests (Anderson Darling, Kolmogorov Smirnov, Lilliefors…) rejected the hypothesis that this distribution came from a normal distribution at a 5 % significance level. However, the number of points was abnormally high because all the points at every depth and every time were considered in the three cases (more than 5 million points in total). But in reality, there were only three “real” points of comparison (*i.e.*, the three boreholes). The Kolmogorov Smirnov statistic was 0.039 and the critical value corresponding at three data points at a 5 % significance level was 0.71, while the critical value with all the points was 10^{-4} order of magnitude. Therefore, in this

context of three "real" points of comparison, the test could not reject the hypothesis that the data came from a normal distribution. Thus, for working with Gaussian uncertainties, we assumed this hypothesis of Gaussian errors and we used the mean error of 0.295°C and the standard deviation (σ) of 0.515 °C (Fig. 5) for our analysis. Based on these results, we systematically removed 0.3 °C (upper bound of 0.295 °C) to the final modeled temperatures and a standard deviation value $\sigma_{Cryogrid}$ = 0.55 °C (upper bound of 0.515 °C) was considered for uncertainty (as a reminder, σ corresponds to a 68 % reliable level and 2σ to a 95 % reliable level for Gaussian data).

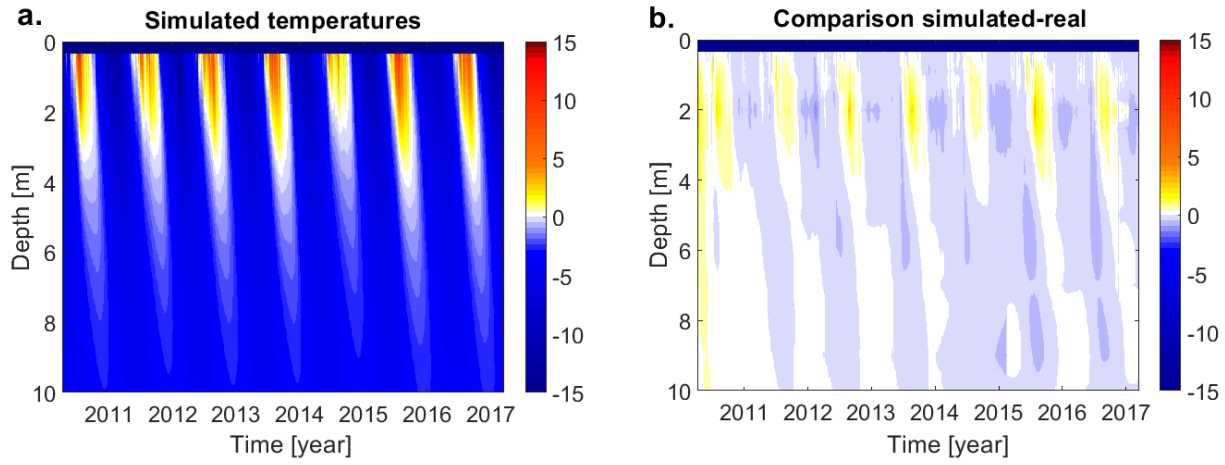

Figure 4. a. BH_E borehole simulation realized with parameters detailed in Table 2. Input surface temperatures were extracted from the borehole real values. The 0.3 m spatial shift at the top of the profiles is due to the depth of the first temperature value recorded in the borehole. **b.** Comparison between BH_E borehole simulation and real BH_E borehole values. RMSE can then be displaced from these values $(e_i)_{i\in[1:N]}$ by the following formula: $RMSE = \sqrt{\frac{\sum_{i=1}^{N} e_i^2}{N}}$.

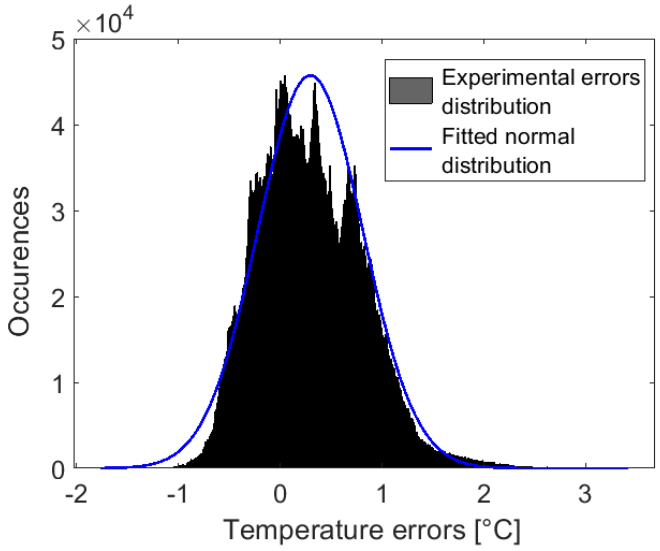

241

242 **Figure 5.** Fit of the temperature errors by a normal distribution. Errors are defined as the difference between the
243 simulated borehole temperatures (BH_S, BH_E or BH_N) and the real borehole temperatures. The fit gave a mean of
244 0.295 °C and a standard deviation of $\sigma = 0.515$ °C.

245 *3.4. Uncertainty analysis*

246 In addition to the uncertainty associated with model parameters, the uncertainty of the forcing RST
247 time series must be considered. RST time series being created as the summation of a MARST and
248 anomaly values (see sect. 3.2.), we consider two terms for this uncertainty, one for the MARST
249 and one for the anomalies. For the MARST, the standard deviation of 1.616 °C is reported in the
250 study from Boeckli et al.[51] that describes the statistical model on which is based the initial MARST
251 used in our study (displayed in Fig. 1). We thus kept the upper bound of this value to determine
252 $\sigma_{MARST} = 1.7$ °C. For the anomalies, the uncertainty results from the only consideration of the air
253 temperature changes in Chamonix to create RST anomalies while daily RST variations may also
254 result of the varying lapse rate, which is typical of alpine environments[54], as well as the varying
255 incoming solar radiation and possible snow accumulation[49] which are neglected. We calculated
256 the uncertainty for RST anomalies, referred as $\sigma_{anomaly}$, by using a set of measured RST time series

at 5 sensors installed at the top of the ADM in sub-vertical S (2 sensors), N, E, and W exposed rock faces, at a depth of 0.03 m[49].

One of the two S-exposed sensors is located right above a ledge where snow accumulates during winter which lowers the MARST by about 1°C compared to snow-free conditions for similar sun-exposure[49]. RST have been recorded continuously at an hourly time step from 2007 to 2010. The MARST for the years 2007 to 2010 were then calculated for each sensor and were adjusted to the 1961-1990 period by applying the air temperature anomaly between 1961-1990 and the years of measurements (2007 to 2010). Then, the adjusted MARST of each sensor was subtracted to the measured daily RST to obtain daily temperature anomalies at sensor locations.

Comparison between the daily air temperature anomalies measured in Chamonix and the RST anomalies calculated from the 5 RST sensors resulted in Gaussian errors with a standard deviation of $\sigma_{anomaly}$ = 4 °C.

To sum up, the uncertainties were as follows:

- $\sigma_{Cryogrid}$ = 0.55 °C
- σ_{MARST} = 1.7 °C
- $\sigma_{anomaly}$ = 4 °C

Then, for surface temperature series, the total uncertainty was:

$$\sigma_{surf} = \sqrt{\sigma_{MARST}^2 + \sigma_{anomaly}^2} \qquad (2)$$

Numerically, it gave: σ_{surf} = 4.4 °C.

In the next part of the study, the temperature at the depth of the rockfall scar was analyzed (referred hereafter as “scar temperature”). With most scar depth > 1 m (Tab. 1), these temperatures were not significantly affected by daily surface temperature changes. Thus, $\sigma_{anomaly}$ was neglected when dealing with scar temperatures and total uncertainty for scar temperature was therefore:

$$\sigma_{\text{scar}} = \sqrt{\sigma_{\text{Cryogrid}}^2 + \sigma_{\text{MARST}}^2} \qquad (3)$$

Numerically, it gave: σ_{scar} = 1.8 °C.

To analyze the results, we also used temperature percentiles (sect. 4). A X % temperature percentile is defined as a value which is warmer than X % and colder than (100-X) % of some chosen reference temperatures which were defined as explained in section 4. To estimate modeled temperature percentile uncertainties, simulations were done for the three boreholes, using the MARST map (Fig. 1) and the air temperature anomaly to generate the forcing surface temperature time series. Percentiles of the modeled temperature values were then calculated for the full borehole time series and compared with the real temperature percentile values. Gaussian errors were obtained, with $\sigma_{surf\ prct}$ = 13.8 % and $\sigma_{scar\ prct}$ = 10.7 %. This approach of considering all the uncertainty sources at once was less precise but sufficient in that case with long and complex calculations.

3.5. Approach for simulating the temperature dynamics at rockfall locations

To analyze bedrock thermal dynamics prior to rockfalls, the following protocol was used for every event:

- The rock surface temperature time series was created as described in section 3.2.
- The CryoGRID2 simulations were run between 1st January 1993 and 31st December 2015, with the bedrock parameters determined after fitting (Tab. 2). Given that the fitting step showed that a spin-up period of 3 years is sufficient, we assumed that the years 1993-1996 were the spin-up years while rockfalls are only documented since 2007. The simulated T_z profiles were 20.5 m long, which is 5 m deeper than the deepest scar depth (Tab. 1). This

300 5 m buffer permitted to lower the errors in the deeper part of the profiles where the
301 correction thermal flux was applied (see sect 3.3).

302 This process was entirely automated in Bash language and MATLAB programs on the Univ.
303 Savoie Mont Blanc - CNRS/IN2P3 MUST computing center. Then, all the simulations could be
304 started at the same time on different calculation resources.
305
306 ## 4. Approach for result analysis
307 ### *4.1. Model output processing and analysis*

308 Four rock temperature variables were analyzed: the (i) scar and (ii) surface temperatures, and the
309 (iii) scar and (iv) surface temperature percentiles. They were all examined through 11 different
310 temporalities: 1 day, 3 days, 5 days, 1 week, 10 days, 2 weeks, 17 days, 3 weeks, 1 month, 45 days
311 and 2 months. The surface temperature was simply extracted at the uppermost depth of the T_z
312 profile (0.05 m). The scar temperature was extracted at the scar depth specified in the rockfall
313 database for each event (Tab. 1). For temporality of 1 day, surface temperature percentiles were
314 calculated by comparing the simulated surface temperature at the day of rockfall occurrence with
315 all the daily surface temperatures of the simulated time series (1st January 1996 - 31st December
316 2015). For other temporalities of *n* days prior to rockfall occurrence, the reference temperatures
317 were calculated by averaging the temperature between a day *d1* which is, by turns, each day in the
318 temperature time series, and a day *d0* which is the first day of the averaging period prior to *d1*,
319 defined as $d0 = d1 - n + 1$. Then, the average temperatures for the various temporalities prior to
320 failure were compared with the respective reference temperatures. At this step, we had only
321 absolute values of surface and scar temperatures, and absolute values of surface and scar

322 temperature percentiles. We then aimed at answering if this temperature value was abnormally
323 high for the current period.
324 To do so, 1000 dates were drawn randomly and the 4 studied variables were extracted for the 11
325 different temporalities at each rockfall location. The choice of the number of random events was
326 based on a compromise between the calculation resources and the potential to reduce the
327 uncertainty. The scar depths of the 1000 random dates of a specific event location were chosen
328 equal to the scar depth of this event. To remove sources of biases, dates of the random events were
329 drawn: a) after 2007 and b) with the same monthly distribution as the 209 rockfalls events. Reason
330 for a) was to remove biases linked to the recent decades of atmospheric warming as the rockfall
331 database starts in 2007. If artificial rockfall events would have been drawn in the full period 1996-
332 2015, extracted temperatures at the beginning of the time series would have been expected to be
333 lower and it would have been impossible to determine if a significance of warmer temperatures
334 for rockfall events was real or just related to the atmospheric warming contribution. Reason for b)
335 is that rockfalls mostly occurred between June and October (with an attendance peak in August,
336 Fig. 6a) and these months were, on average, warmer than other months of the year. If random
337 events would have been drawn in the full year, a significance of warmer temperature for real events
338 could have been simply interpreted as the reflection of this reason and not as an extraordinary
339 thermal state of the rock before the failure. Thus, random events were drawn according to the same
340 monthly distribution as the 209 real events (Fig. 6a). Figure 6b shows that the temporal distribution
341 of rockfall events is not dependent on the scar depth, that is why the same monthly distribution is
342 taken for every scar depth and that no scar depth groups were created. Likewise, no relationship
343 was found with the elevation, the slope angle or the sun-exposure (Fig. S1).
344

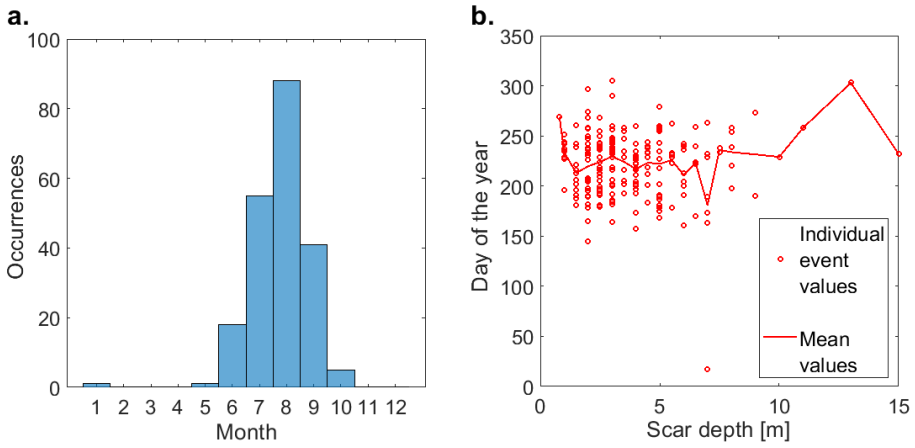

Figure 6. a. Histogram illustrating the distribution of the 209 rockfalls throughout the year that was used as a basis to draw random events dates. **b.** Plot illustrating the distribution of the events throughout the year in comparison to the scar depths. The absence of relationship between scar depth and rockfall timing was considered to not draw the monthly distribution of random events according to depth. The same is true for elevation, slope angle and sun-exposure (Fig. S1). Means of 0.8 m, 9 m, 10 m, 11 m, 13 m and 15 m scar depths must be observed carefully because they are represented by one or two points only.

4.2. *Determining results significance*

For searching significant results, real rockfalls temperatures and temperature percentiles were compared with those of random events. Firstly, a simple comparison of the means for every scar depth and every temporality was realized. Then, the comparison was done for every temporality without regarding the scar depth. Uncertainties were derived by dividing the uncertainty of the variable (σ_{surf}, σ_{scar}, $\sigma_{surf\ prct}$ or $\sigma_{scar\ prct}$) by the square root of the total number of points used for calculating the mean. Since 209 000 random events were considered, uncertainties of the means of random events variables were small and almost impossible to see when plotted against the real events uncertainty.

A Kolmogorov Smirnov test (KS test) was then performed for assessing if the real rockfalls sample could have been drawn from the random events distribution. It was calculated by determining the highest ordinate difference between the Cumulative Distribution Functions (CDFs) of the real rockfalls and the random events series. This statistic was then compared with tabulated critical values for obtaining the result of the test. This test was chosen because it is non-parametric, which is important since the temperature percentiles are clearly not Gaussian (Anderson Darling, Kolmogorov Smirnov and Lilliefors tests reject this hypothesis with a 5 % significance level), and because it was possible to consider the uncertainty values while performing the test. This second point is, astonishingly and unfortunately, uncommon for statistical tests. The only feasible rough uncertainty incorporation is generally to present upper and lower bounds of the test by realizing it with the high and low values of the data points. Here, for surface or scar temperature percentiles, the uncertainties were included as explained in the Supplement S2.

An example of CDF represented with the uncertainties and resulting KS test is displayed in Figure 7 for one specific variable (surface temperature percentile) and one specific temporality (1 day). The KS statistic must be compared with the critical value (cv). If the statistic is higher, the test rejects the hypothesis that the experimental data (real events) comes from the model (random events) with a 5 % significance level. Here, the test rejected the hypothesis that the experimental data (real events) came from the model (random events) in the normal case with a 5 % significance level, but could not reject this hypothesis when considering the uncertainties.

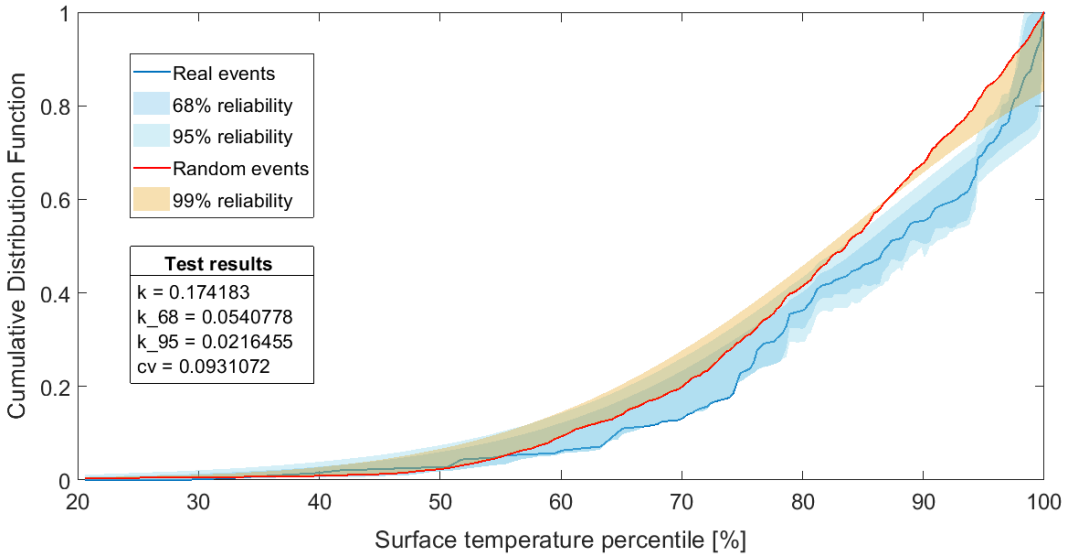

Figure 7. Illustration of a KS test result. The surface temperature percentiles were here considered at the rockfall event day (temporality of 1 day). "k" represents the KS statistic between the CDFs without considering the uncertainties. "k_68" represents the statistic between the 68 % reliable real events CDF and the 99 % reliable random events CDF. "k_95" represents the statistic between the 95 % reliable real events CDF and the 99 % reliable random events CDF. The 68 % and 95 % reliable random events CDFs are not presented because they were very close to the 99 % reliable one (the reason for this stability is that random events CDF is made of 209 000 points). "cv" is the 5 % significance level critical value of the KS test in this context. To know the result of the test, the KS statistic must be compared with the critical value. If the statistic is higher, the test rejects the hypothesis that the experimental data (real events) come from the model (random events) with a 5 % significance level. Here, the test rejected the hypothesis in the normal case but could not reject it when considering the uncertainties.

To show orders of magnitude of simulated temperatures, scar and surface temperature variables were used in a first step. However, in a second step, only temperature percentile variables were kept since they are better for finding statistical significance.

5. Results

When considering the uncertainties, none of the four variables (surface and scar depth temperatures and temperature percentiles) could be distinguished from the random events values when reasoning by scar depth. This finding is illustrated in Figure 8 for a temporality of 1 day while other temporalities, showing similar patterns, are displayed in the Supplements (Fig. S2). However, whatever the considered variable, the mean distributions were in most cases - except 6 and 7 m depths - higher than the random events. This was particularly pronounced for the percentile variables. The four variables were strikingly scattered, but some notable patterns could be distinguished. First, the closer to the surface, the warmer was the scar temperature, for both real and random events. The average temperature became negative from 3-4 m depth downward (see Fig. S2 also) but consistency in negative scar temperature was found for depths > 6 m only, despite a few events showed positive and close to 0 °C conditions. Only 2 events had scar temperature < -5 °C. The surface temperatures were mostly positive and no distinct pattern could be found according to scar depths. Scar temperature percentiles scattering increased with depth and their mean decreased from 90 to 50 % between 1 and 9 m depth while surface temperature percentiles showed no obvious link with scar depths. When extending the temporalities (Fig. S2), very similar patterns were found, with slightly smaller scattering, slightly higher surface percentiles and slightly lower scar temperature percentiles.

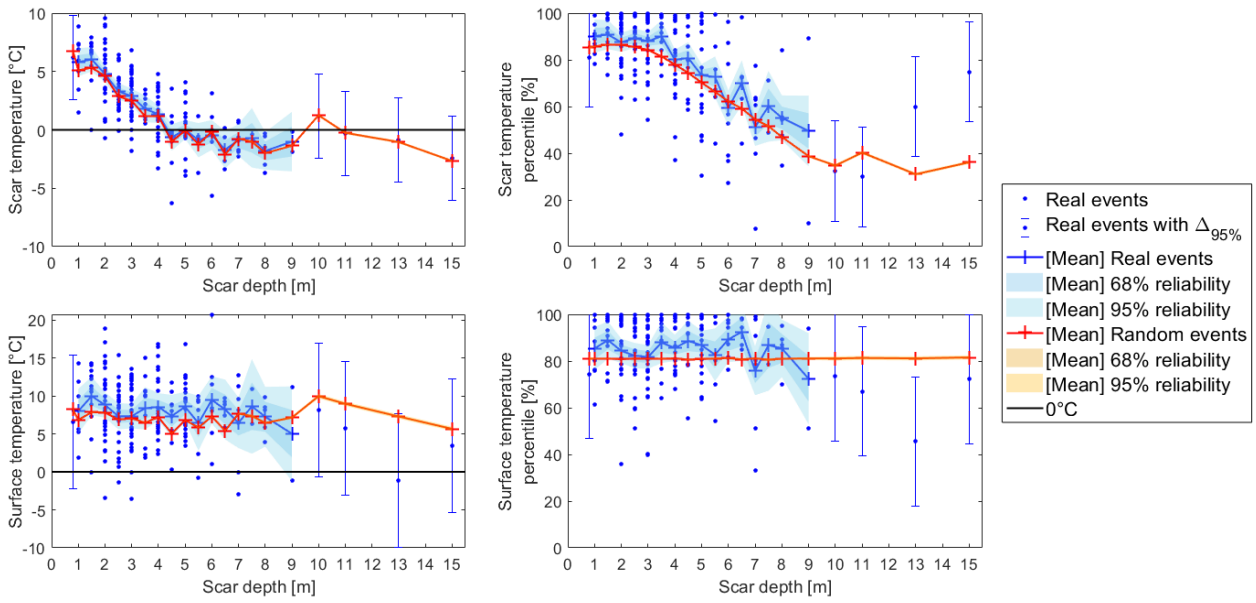

Figure 8. Comparison of the four studied variables between real and random rockfalls on the day of the event (temporality of 1 day). This comparison was done for every scar depth, all the events with the corresponding value of scar depth being used for calculating a mean. Ten other groups of figures like this one were done to verify our results for the 10 other temporalities (3 days, 5 days, 1 week, 10 days, 2 weeks, 17 days, 3 weeks, 1 month, 45 days and 2 months) and four of them (1 week, 2 weeks, 1 month and 2 months) are presented in the Supplements (Figures S2). Uncertainties of random events variables cannot be seen because they were really low (order of magnitude of some degree tenths for temperature variables and some percent tenths for temperature percentile variables).

When looking at the results through the different temporalities, percentiles of scar and surface temperatures were, distinctively higher than the random events values, whatever the temporality (Fig. 9). For scar temperature percentiles, this difference was in order of magnitude of 3 % for mean values and at least 1.5 % for 95 % reliability values. For surface temperature percentiles, these percentages were nearly equal to 2.5 and 0.5 %.

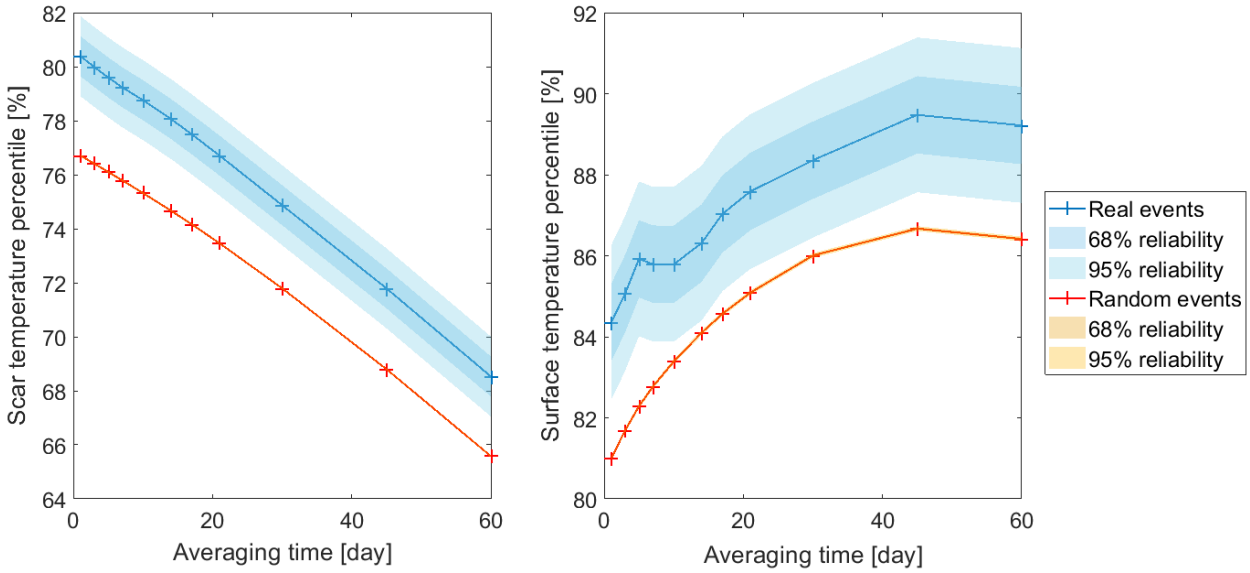

Figure 9. Comparison of the average temperature percentile variables between real and random rockfalls. Here, all scar depths were merged which explains a constant and rather low uncertainty (individual uncertainty divided by the square root of the total number of events, 209 for the real ones and 209 000 for the random ones). Every single point of this represents a full plot of Figure 8.

Implementation of the KS test showed that scar temperature percentiles for real events were significantly different from random events for temporalities between 1 and 21 days (Fig. 10). This significance decreases almost continuously with increasing temporality. Surface temperature significances varied with the different temporalities but were always well above the critical threshold. It reached its minimum value at about 14 days averaging time prior to failure and then increased continuously until 45 days averaging time prior to failure where it reached its maximum value. However, when considering the uncertainty, these results were not significant and it was therefore not possible to state whether the real events sample could have been drawn from the random events distribution. This points out the interest to work with a greater number of rockfalls.

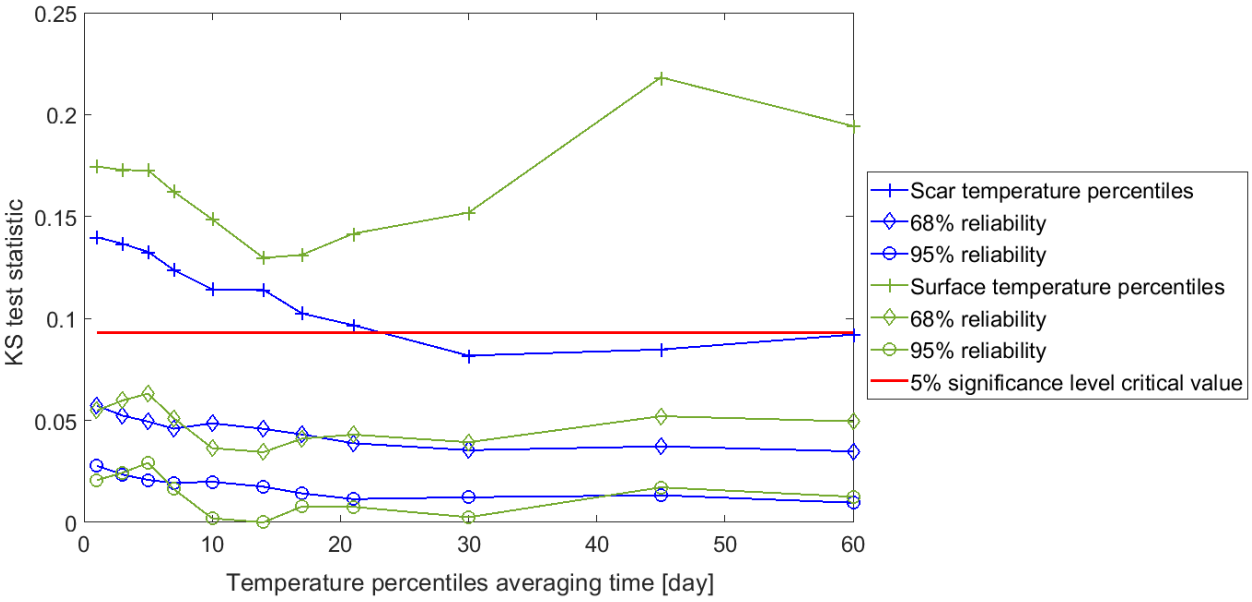

Figure 10. Illustration of the significance of scar and surface temperature percentiles for every temporality. Every point of this plot corresponds to a KS test. For example, the three values "k", "k_68" and "k_95" calculated in Figure 7 are here represented by the green triplet of points (plus-sign marker, diamond marker and circular marker) at the 1-day abscissa.

6. Discussion

6.1.Strengths and limitations of the study

For this study, we have used a homogeneous rockfall inventory which ensures direct comparability of the results and a coherent statistical analysis. The relatively simple thermal modeling approach may appear as the main limitation since it lacks of consideration for solar radiation variability through time, precipitations and wind effects, or snow deposit controls. Energy balance approaches which have been commonly used in rockwall permafrost modeling[19,55–57] would allow overcoming some of these limitations. However, by introducing a greater number of input parameters, energy balance models bear numerous sources of uncertainty, challenging its quantification[58]. In this way, our simple modeling approach combined with the availability of bedrock temperature data into

463 boreholes has the main advantage to permit a detailed uncertainty analysis of our results. In
464 addition, our approach accounts for most important parameters which are an average value of
465 incoming short-wave solar radiation and air temperature (for the MARST calculation[59]) at the
466 bedrock surface and the heat conduction at depth. Nevertheless, bedrock thermal parameters
467 (conductivity and heat capacity) have been calibrated with borehole temperature measurements
468 collected in the granitic part of the MBM while 18 (8.6 %) of the rockfalls occurred in the
469 metamorphic series. But since these series have in most cases very similar mineral composition as
470 the granitic unit[47], it is assumed that the results are marginally impacted, the variable anisotropy
471 which is not only related to lithology but also to site-specific fracturing possibly being the most
472 critical issue.
473 Another limit lies in snow deposits that may cool the bedrock surface and delay the thawing onset
474 during warm seasons[57,60] when some rockfalls occurred. Thus, the greater statistical significance
475 of rather long time period of high surface temperature prior to rockfalls may partly depict the time
476 needed for snow melt for some events. But, in parallel, snow melt or rainfalls could also accelerate
477 the thawing through water percolation into bedrock fractures[30,32]. The only possible reflection of
478 this overlooked effect in the results would be the events with rather low scar temperature
479 percentiles right before failure (Fig. 8). This means that the bedrock temperature didn't reach its
480 highest value when the failure occurred suggesting either that sudden heating is not the main
481 triggering factor or that other processes such as heat advection may have locally accelerated
482 bedrock warming. Such accelerated bedrock thawing was already suggested by former studies[19,37]
483 to explain permafrost-related rockfalls. Despite these limits, our results allow discussing possible
484 thermal processes triggering rockfalls according to scar depth and climate signal characteristics.
485

6.2. Results interpretation

The role of thermal processes in rockfall triggering

Variables comparison with scar depths (Fig. 8) has shown that it would have been irrelevant to analyze the results based on scar depth groups. Such an analysis could have been attractive since it could have been expected that scar temperature significance would have overweighted the one of surface temperature. But the constantly low difference between random and real events variables shows that the observed pattern is not specific to the real events and that the supposedly link between scar depth and bedrock temperature pattern must be seen as the depiction of general thermal conditions at rockfall locations. The decreasing average in scar variables (Fig. 8) must be seen as the expected depth effect involving a delayed response to climate signals.

Temperature values at scar depths discriminate possible rockfall triggering processes with permafrost degradation or frost-related processes strongly suggested for events > 6 m and for a significant part of shallower events (3 to 6 m). On average, these events occurred in a range of temperature between 0 and -2 °C and show noticeable agreement with experimental and theoretical knowledge about reduced shear strength of ice-filled fractures within this temperature range[24,27]. In mountain environments, rockwalls are prone to instability because of extreme conditions with large and sometimes sudden temperature variation, freeze and thaw cycles, as well as wet and dry cycles throughout the year[29,61–64]. Frost weathering processes related to ice segregation and volumetric expansion, as well as repeated freeze and thaw cycles leading to bedrock fatigue are well recognized mechanisms preparing to bedrock failures by breaking rock bridges and favoring fracture propagation[61,65–67]. Similarly, high thermal stress related to strong thermal oscillations is also regarded as an essential factor favoring bedrock cracking due to repeated thermal contractions and expansions that also affect non-periglacial rockwall, the warm days being particularly prone

to rockfall occurrence[39,40,68,69]. The fact that many shallow events occurred at positive rock temperature but also well higher than average rock temperatures as suggested by the temperature percentiles, corroborates those studies.

In addition to the interpretation of possible processes acting in rockfall, percentiles reveal how air temperature signals contribute to their triggering. Indeed, temperature values are suited for an intrinsic comparison of the rockfall sample elements, while temperature percentiles rather inform about the thermal dynamics specific to each location of the rockfall sample elements. In addition, percentiles are better suited for determining statistical significance.

Link between air temperature signals and rockfall triggering

Comparisons of percentile means (Fig. 9) show that the real events have, in average, a warmer temperature condition prior to failure than random ones, whatever the considered temporality, from 1 day to 2 months (Fig. 8 and S2). However, the difference between the real rockfall events and the random rockfall events can also be a statistical "sample effect" and the questions of whether and to what extent the sample could have been drawn from the model persist. This question is answered by the KS test and the significance study (Fig. 10). In the following, a high significance must be interpreted as an approval of the previous results, namely that the real events show warmer temperature conditions than usual and that this difference is not due to a "sample effect". The results show that the surface temperature percentiles between 1 day and 2 months prior to failure are significantly higher than usual. More specifically, the highest significance for these exceptionally high surface temperature percentiles is found 1.5 to 2 months prior to failure and, in to a lesser extent, at an early time prior to the rockfall (1 to 5 days). In between these early and late time periods, the statistical significance for the surface temperature percentiles decreases

and reaches a minimum at 2 weeks. This suggests that rockfall occurrences are favored by long-lasting heatwaves (*i.e.* extended period of unusually high atmospheric heat) overtopped by a hot spell (one or a few days of intense heat)[70]. This early compound can thus be interpreted as a triggering effect which only reinforces a long-term high surface temperature signal. The late compound becomes more relevant in relation to the statistical significance of the scar temperature temporalities. Indeed, high significances of scar temperatures for short time period (< 20 days) are in some ways a corollary of high percentiles of surface temperature for at least a month due to the delay needed for heat diffusion. But this would mean that bedrock failures are somewhat a direct response to extraordinary high temperature at depth. Such results are partly in agreement with the findings from Luethi et al.[37]. This last study found that mid-sized rockfalls such as those we investigated are a direct response to short-term periods of high surface temperature. The authors attribute this fast reaction to accelerated bedrock thawing provoked by advective heat transfer from water percolation. While this study was not accounting for the thermal dynamics at scar depth, our study shows that scar depths were also affected by exceptionally high temperatures which are explained by the only effect of heat conduction. It further demonstrates that this high temperature at scar depth is likely a response to several weeks or months of high bedrock surface temperature. It does not exclude effect of advective heat transport but suggests that heat conduction exerts a predominant control. Such findings somehow remind the findings from Paranunzio et al.[36] which pinpointed warm air temperature anomaly associated with a majority of rockfalls observed in the Western Italian Alps. Finally, similarly to the study of Luethi et al.[37], it confirms that other thermal processes than permafrost degradation are probably responsible for small size rockfalls, supposedly high thermal stress due to intense temperature variation favoring bedrock failure preparation.

These interpretations must be considered with caution since they are based on findings for which the significance cannot be confirmed when considering the modeling approach uncertainty. This limit draws some research outlooks that could lead to the definition of a susceptibility index of a rockfall to occur according to the weather forecast.

6.3. Outlooks

Our study has shown that when considering model uncertainty, a part of our interpretation loses significance as it is not clear whether the same results could have been drawn from a random sample. For lowering these uncertainties and confirming/improving these results, two solutions are possible.

The first one, which is the most challenging, is to lower the modeled temperature uncertainties ($\sigma_{Cryogrid}$, σ_{MARST} or $\sigma_{anomaly}$; see sect. 3.5). $\sigma_{Cryogrid}$ could be improved by getting other borehole data in order that CryoGRID2 parameters better represent the study area (boreholes in rockwalls with other characteristics or in the metamorphic basement for example). σ_{MARST} could be tackled by modeling the MARST with a RST sample collected in the study area rather than across the entire European Alps[35,51]. Finally, $\sigma_{anomaly}$ could be improved by better defining the daily surface temperature (see sect. 3.2.). RST anomaly time series could be created at the specific rockfall locations by combining different meteorological parameters in a well-constrained energy balance model.

The second solution for lowering the uncertainties would be to increase the sample size with a higher number of rockfalls. This would lower the KS test critical values and the CDF uncertainties. This second solution would be considered in the near future as the rockfall database will be enriched with more recent events (2016-2020) which are currently under processing.

Additionally, with the method described in sect. 4, atmospheric warming and seasonal biases have been ruled out. However, the bias linked with the rockfall locations persists. Indeed, the studied locations were possibly particularly prone to instability (fracturing for example) as much as rockfall dates were favorable for example. For removing this bias, random events should be chosen in all the MBM, with characteristics (altitude, exposure, slope angle…) in accordance with the rockfall sample characteristics. Such a study, in the continuation of this work, could result in the development of a rockfall susceptibility index. This index would be defined with the values of the four variables presented and, particularly, with their significances. This work of gathering all this information could be done by machine learning or deep learning. Some of the real events will be used in the learning process and the others for the testing step. Such a rockfall susceptibility index could be a preliminary step towards a direct societal contribution of the past decade of permafrost research, supporting risk mitigation and public awareness in a rapidly evolving environment.

7. Conclusions

In this paper, the thermal conditions and dynamics at and prior to rockfalls have been analyzed for 209 events inventoried in the MBM between 2007 and 2015 with 1D temperature modeling. Using temperature measurements at five locations at the rock surface and into three 10-m-deep boreholes, model uncertainty was quantified to refine model interpretation. Based on a random events analysis approach, recent decades of atmospheric warming and seasonal biases have been removed, and the statistical significance of our results was determined. The results were analyzed through surface and scar depth temperature values to discriminate possible processes responsible for rockfall triggering, as well as through temperature percentiles to analyze the statistical

601 significance and whether the rockfalls are a direct reaction to extreme air temperature signals.
602 Percentiles were defined in relation to 11 temporalities ranging from 1 day to 2 months. KS tests
603 were performed to determine whether our results could have been found from the random sample.
604 Our study draws the following conclusions:

605 ● Permafrost degradation may be responsible for almost all events which scar depth was >
606 6 m, and for a significant part of events occurring between 3 and 6 m depth.

607 ● For the 209 real events, the surface and scar temperature percentiles were, on average,
608 warmer than those of the random events. This difference is present for all the considered
609 temporalities. It is in order of magnitude of 3 % for scar temperature percentiles (1.5 % at least at
610 95 % reliability level) and 2.5 % for surface temperature percentiles (0.5 % at least at 95 %
611 reliability level).

612 ● KS test shows significant relationships between rockfalls and surface temperature
613 percentiles at least up to 2 months prior to failure, and scar temperature percentiles up to 3 weeks
614 before the events. At the rock surface, temporalities > 1 month have the greatest significance and
615 those of 1-5 days are also remarkable. At scar depths, the closer to the event day, the greater the
616 significance.

617 ● Significance results are interpreted as the effects of 1 to 5 days of extraordinary hot
618 weather (hot spell) acting as a triggering mechanism after > 1 month of exceptionally high air
619 temperature (long lasting heatwave), which result in high temperature at depth and sudden bedrock
620 failure.

621 ● Decrease of the scar temperature percentiles significances suggests that rockfalls are a
622 direct reaction (lasting less than 3 weeks) to exceptionally high bedrock temperature.

623 ● When considering 95 % reliability level, uncertainties are too high for concluding
624 anything about KS test significances (the three last points).
625 ● Our study also points out the interest to apply such an approach with a greater rockfall
626 sample to better define the significance levels and appears promising to develop rockfall
627 susceptibility index using weather forecast.
628
629

630 **8. Acknowledgments**

631

632 This work has been done thanks to the facilities offered by the Univ. Savoie Mont Blanc -
633 CNRS/IN2P3 MUST computing center. We acknowledge S. Westermann from the University of
634 Oslo for providing the CryoGRID model code. This work was supported by the ANR-19-CE01-
635 0018 WISPER.

636

637 **9. References**

638 1. Ravanel L, Allignol F, Deline P, Gruber S, Ravello M. Rock falls in the Mont Blanc Massif
639 in 2007 and 2008. *Landslides*. 2010;7(4):493-501. doi:10.1007/s10346-010-0206-z

640 2. Haeberli W, Wegmann M, Vonder Mühll D. Slope stability problems related to glacier
641 shrinkage and permafrost degradation in the Alps. 1997;(90):407-414.

642 3. Ravanel L, Deline P, Lambiel C, Vincent C. Instability of a High Alpine Rock Ridge: the
643 Lower Arête Des Cosmiques, Mont Blanc Massif, France. *Geogr Ann Ser Phys Geogr*.
644 2013;95(1):51-66. doi:10.1111/geoa.12000

645 4. Duvillard P-A, Ravanel L, Marcer M, Schoeneich P. Recent evolution of damage to
646 infrastructure on permafrost in the French Alps. *Reg Environ Change*. Published online
647 February 11, 2019. doi:10.1007/s10113-019-01465-z

5. Bommer C, Institut fédéral de recherches sur la forêt la neige et le paysage (Birmensdorf). *Construire sur le pergélisol: guide pratique*. Institut fédéral de recherches sur la forêt, la neige et le paysage WSL; 2010.

6. Purdie H, Gomez C, Espiner S. Glacier recession and the changing rockfall hazard: Implications for glacier tourism. *N Z Geogr*. 2015;71(3):189-202. doi:10.1111/nzg.12091

7. Mourey J, Marcuzzi M, Ravanel L, Pallandre F. Effects of climate change on high Alpine mountain environments: Evolution of mountaineering routes in the Mont Blanc massif (Western Alps) over half a century. *Arct Antarct Alp Res*. 2019;51(1):176-189. doi:10.1080/15230430.2019.1612216

8. Huggel C, Zgraggen-Oswald S, Haeberli W, et al. The 2002 rock/ice avalanche at Kolka/Karmadon, Russian Caucasus: assessment of extraordinary avalanche formation and mobility, and application of QuickBird satellite imagery. *Nat Hazards Earth Syst Sci*. 2005;5(2):173-187. doi:https://doi.org/10.5194/nhess-5-173-2005

9. Carey M. Living and dying with glaciers: people's historical vulnerability to avalanches and outburst floods in Peru. *Glob Planet Change*. 2005;47(2):122-134. doi:10.1016/j.gloplacha.2004.10.007

10. Walter F, Amann F, Kos A, et al. Direct observations of a three million cubic meter rock-slope collapse with almost immediate initiation of ensuing debris flows. *Geomorphology*. 2020;351:106933. doi:10.1016/j.geomorph.2019.106933

11. Allen SK, Rastner P, Arora M, Huggel C, Stoffel M. Lake outburst and debris flow disaster at Kedarnath, June 2013: hydrometeorological triggering and topographic predisposition. *Landslides*. 2016;13(6):1479-1491. doi:10.1007/s10346-015-0584-3

12. Haeberli W, Huggel C, Kääb A, et al. The Kolka-Karmadon rock/ice slide of 20 September 2002: an extraordinary event of historical dimensions in North Ossetia, Russian Caucasus. *J Glaciol*. 2004;50(171):533-546. doi:10.3189/172756504781829710

13. Huggel C, Allen S, Deline P, Fischer L, Noetzli J, Ravanel L. Ice thawing, mountains falling—are alpine rock slope failures increasing? *Geol Today*. 2012;28(3):98-104. doi:10.1111/j.1365-2451.2012.00836.x

14. Fischer L, Purves RS, Huggel C, Noetzli J, Haeberli W. On the influence of topographic, geological and cryospheric factors on rock avalanches and rockfalls in high-mountain areas. *Nat Hazards Earth Syst Sci*. 2012;12(1):241-254. doi:https://doi.org/10.5194/nhess-12-241-2012

15. Ravanel L, Deline P. Climate influence on rockfalls in high-Alpine steep rockwalls: The north side of the Aiguilles de Chamonix (Mont Blanc massif) since the end of the 'Little Ice Age.' *The Holocene*. 2011;21(2):357-365. doi:10.1177/0959683610374887

16. Deline P, Gardent M, Magnin F, Ravanel L. The Morphodynamics of the Mont Blanc Massif in a Changing Cryosphere: A Comprehensive Review. *Geogr Ann Ser Phys Geogr*. 2012;94(2):265-283. doi:10.1111/j.1468-0459.2012.00467.x

17. Allen SK, Gruber S, Owens IF. Exploring steep bedrock permafrost and its relationship with recent slope failures in the Southern Alps of New Zealand. *Permafr Periglac Process*. 2009;20(4):345-356. doi:10.1002/ppp.658

18. Allen SK, Cox SC, Owens IF. Rock avalanches and other landslides in the central Southern Alps of New Zealand: a regional study considering possible climate change impacts. *Landslides*. 2011;8(1):33-48. doi:10.1007/s10346-010-0222-z

19. Gruber S, Hoelzle M, Haeberli W. Permafrost thaw and destabilization of Alpine rock walls in the hot summer of 2003. *Geophys Res Lett*. 2004;31(13). doi:10.1029/2004GL020051

20. Ravanel L, Magnin F, Deline P. Impacts of the 2003 and 2015 summer heatwaves on permafrost-affected rock-walls in the Mont Blanc massif. *Sci Total Environ*. 2017;609:132-143. doi:10.1016/j.scitotenv.2017.07.055

21. Deline P, Broccolato M, Noetzli J, Ravanel L, Tamburini A. The December 2008 Crammont Rock Avalanche, Mont Blanc Massif Area, Italy. In: Margottini C, Canuti P, Sassa K, eds. *Landslide Science and Practice: Volume 4: Global Environmental Change*. Springer; 2013:403-408. doi:10.1007/978-3-642-31337-0_52

22. Frauenfelder R, Isaksen K, Lato MJ, Noetzli J. Ground thermal and geomechanical conditions in a permafrost-affected high-latitude rock avalanche site (Polvartinden, northern Norway). *The Cryosphere*. 2018;12(4):1531-1550. doi:https://doi.org/10.5194/tc-12-1531-2018

23. Deline P, Gruber S, Delaloye R, et al. Chapter 15 - Ice Loss and Slope Stability in High-Mountain Regions. In: Shroder JF, Haeberli W, Whiteman C, eds. *Snow and Ice-Related Hazards, Risks and Disasters*. Academic Press; 2015:521-561. doi:10.1016/B978-0-12-394849-6.00015-9

24. Krautblatter M, Funk D, Günzel FK. Why permafrost rocks become unstable: a rock–ice-mechanical model in time and space. *Earth Surf Process Landf*. 2013;38(8):876-887. doi:10.1002/esp.3374

25. Gruber S, Haeberli W. Permafrost in steep bedrock slopes and its temperature-related destabilization following climate change. *J Geophys Res Earth Surf*. 2007;112(F2). doi:10.1029/2006JF000547

26. Magnin F, Josnin J-Y, Ravanel L, Pergaud J, Pohl B, Deline P. Modelling rock wall permafrost degradation in the Mont Blanc massif from the LIA to the end of the 21st century. *The Cryosphere*. 2017;11(4):1813-1834. doi:https://doi.org/10.5194/tc-11-1813-2017

27. Davies MCR, Hamza O, Harris C. The effect of rise in mean annual temperature on the stability of rock slopes containing ice-filled discontinuities. *Permafr Periglac Process*. 2001;12(1):137-144. doi:10.1002/ppp.378

28. Mamot P, Weber S, Schröder T, Krautblatter M. A temperature- and stress-controlled failure criterion for ice-filled permafrost rock joints. *The Cryosphere*. 2018;12(10):3333-3353. doi:10.5194/tc-12-3333-2018

29. Matsuoka N, Sakai H. Rockfall activity from an alpine cliff during thawing periods. *Geomorphology*. 1999;28(3):309-328. doi:10.1016/S0169-555X(98)00116-0

30. Hasler A, Gruber S, Font M, Dubois A. Advective Heat Transport in Frozen Rock Clefts: Conceptual Model, Laboratory Experiments and Numerical Simulation. *Permafr Periglac Process*. 2011;22(4):378-389. doi:10.1002/ppp.737

31. Krautblatter M, Hauck C. Electrical resistivity tomography monitoring of permafrost in solid rock walls. *J Geophys Res Earth Surf*. 2007;112(F2). doi:10.1029/2006JF000546

32. Phillips M, Haberkorn A, Draebing D, Krautblatter M, Rhyner H, Kenner R. Seasonally intermittent water flow through deep fractures in an Alpine Rock Ridge: Gemsstock, Central Swiss Alps. *Cold Reg Sci Technol*. 2016;125:117-127. doi:10.1016/j.coldregions.2016.02.010

33. Krautblatter M, Huggel C, Deline P, Hasler A. Research Perspectives on Unstable High-alpine Bedrock Permafrost: Measurement, Modelling and Process Understanding. *Permafr Periglac Process*. 2012;23(1):80-88. doi:10.1002/ppp.740

34. Fischer L, Amann F, Moore JR, Huggel C. Assessment of periglacial slope stability for the 1988 Tschierva rock avalanche (Piz Morteratsch, Switzerland). *Eng Geol*. 2010;116(1):32-43. doi:10.1016/j.enggeo.2010.07.005

35. Magnin F, Brenning A, Bodin X, Deline P, Ravanel L. Statistical modelling of rock wall permafrost distribution: application to the Mont Blanc massif. *Géomorphologie Relief Process Environ*. Published online 2015:20.

36. Paranunzio R, Laio F, Chiarle M, Nigrelli G, Guzzetti F. Climate anomalies associated with the occurrence of rockfalls athigh-elevation in the Italian Alps. *Nat Hazards Earth Syst Sci*. 2016;16(9):2085-2106. doi:10.5194/nhess-16-2085-2016

37. Luethi R, Gruber S, Ravanel L. Modelling transient ground surface temperatures of past rockfall events: towards a better understanding of failure mechanisms in changing periglacial environments. *Geogr Ann Ser Phys Geogr*. 2015;97(4):753-767. doi:10.1111/geoa.12114

38. Allen S, Huggel C. Extremely warm temperatures as a potential cause of recent high mountain rockfall. *Glob Planet Change*. 2013;107:59-69. doi:10.1016/j.gloplacha.2013.04.007

39. Bakun-Mazor D, Keissar Y, Feldheim A, Detournay C, Hatzor YH. Thermally-Induced Wedging–Ratcheting Failure Mechanism in Rock Slopes. *Rock Mech Rock Eng*. 2020;53(6):2521-2538. doi:10.1007/s00603-020-02075-6

40. Collins BD, Stock GM. Rockfall triggering by cyclic thermal stressing of exfoliation fractures. *Nat Geosci*. 2016;9(5):395-400. doi:10.1038/ngeo2686

41. Hugentobler M, Loew S, Aaron J, Roques C, Oestreicher N. Borehole monitoring of thermo-hydro-mechanical rock slope processes adjacent to an actively retreating glacier. *Geomorphology*. 2020;362:107190. doi:10.1016/j.geomorph.2020.107190

42. Westermann S, Schuler TV, Gisnås K, Etzelmüller B. Transient thermal modeling of permafrost conditions in Southern Norway. *The Cryosphere*. 2013;7(2):719-739. doi:10.5194/tc-7-719-2013

43. Schär C, Vidale PL, Lüthi D, et al. The role of increasing temperature variability in European summer heatwaves. *Nature*. 2004;427(6972):332-336. doi:10.1038/nature02300

44. Gobiet A, Kotlarski S, Beniston M, Heinrich G, Rajczak J, Stoffel M. 21st century climate change in the European Alps—A review. *Sci Total Environ*. 2014;493:1138-1151. doi:10.1016/j.scitotenv.2013.07.050

45. Christidis N, Jones GS, Stott PA. Dramatically increasing chance of extremely hot summers since the 2003 European heatwave. *Nat Clim Change*. 2015;5(1):46-50. doi:10.1038/nclimate2468

46. Haeberli W, Noetzli J, Arenson L, et al. Mountain permafrost: development and challenges of a young research field. *J Glaciol*. 2010;56(200):1043-1058. doi:10.3189/002214311796406121

47. von Raumer JF, Bussy F. *Mont Blanc and Aiguilles Rouges Geology of Their Polymetamorphic Basement (External Massifs, Western Alps, France-Switzerland)*. Section des Sciences de la Terre, Université de Lausanne; 2004:218. https://www.unil.ch/iste/files/live/sites/iste/files/shared/X.Library/Memoirs%20of%20Geology/42%20-%20Von%20Raumer%20%26%20Bussy%20(2004%20-%20entire%20volume).pdf

48. Gardent M, Rabatel A, Dedieu J-P, Deline P. Multitemporal glacier inventory of the French Alps from the late 1960s to the late 2000s. *Glob Planet Change*. 2014;120:24-37. doi:10.1016/j.gloplacha.2014.05.004

49. Magnin F, Deline P, Ravanel L, Noetzli J, Pogliotti P. Thermal characteristics of permafrost in the steep alpine rock walls of the Aiguille du Midi (Mont Blanc Massif, 3842 m a.s.l). *The Cryosphere*. 2015;9(1):109-121. doi:10.5194/tc-9-109-2015

50. Ravanel L, Deline P. A network of observers in the Mont Blanc massif to study rockfalls in high alpine rockwalls. *Geogr Fis E Din Quat*. 2013;(36):151-158.

51. Boeckli L, Brenning A, Gruber S, Noetzli J. A statistical approach to modelling permafrost distribution in the European Alps or similar mountain ranges. *The Cryosphere*. 2012;6(1):125-140. doi:10.5194/tc-6-125-2012

52. Hasler A, Gruber S, Haeberli W. Temperature variability and offset in steep alpine rock and ice faces. *The Cryosphere*. 2011;5(4):977-988. doi:https://doi.org/10.5194/tc-5-977-2011

53. Noetzli J, Gruber S, Kohl T, Salzmann N, Haeberli W. Three-dimensional distribution and evolution of permafrost temperatures in idealized high-mountain topography. *J Geophys Res Earth Surf*. 2007;112(F2). doi:10.1029/2006JF000545

54. Rolland C. Spatial and Seasonal Variations of Air Temperature Lapse Rates in Alpine Regions. *J Clim*. 2003;16(7):1032-1046. doi:10.1175/1520-0442(2003)016<1032:SASVOA>2.0.CO;2

55. Noetzli J, Gruber S, Kohl T, Salzmann N, Haeberli W. Three-dimensional distribution and evolution of permafrost temperatures in idealized high-mountain topography. *J Geophys Res*. 2007;112(F2):F02S13. doi:10.1029/2006JF000545

56. Luethi R, Gruber S, Ravanel L. Modelling transient ground surface temperatures of past rockfall events: towards a better understanding of failure mechanisms in changing periglacial environments. *Geogr Ann Ser Phys Geogr*. 2015;97(4):753-767. doi:10.1111/geoa.12114

57. Magnin F, Westermann S, Pogliotti P, Ravanel L, Deline P, Malet E. Snow control on active layer thickness in steep alpine rock walls (Aiguille du Midi, 3842ma.s.l., Mont Blanc massif). *CATENA*. 2017;149:648-662. doi:10.1016/j.catena.2016.06.006

58. Loucks DP, Beek E van, Stedinger JR. *Water Resources Systems Planning and Management: An Introduction to Methods, Models and Applications*. UNESCO; 2005.

59. Magnin F, Brenning A, Bodin X, Deline P, Ravanel L. Modélisation statistique de la distribution du permafrost de paroi : application au massif du Mont Blanc. *Géomorphologie Relief Process Environ*. 2015;21(vol. 21 – n° 2):145-162. doi:10.4000/geomorphologie.10965

60. Magnin F, Deline P, Ravanel L, Noetzli J, Pogliotti P. Thermal characteristics of permafrost in the steep alpine rock walls of the Aiguille du Midi (Mont Blanc Massif, 3842 m a.s.l). *The Cryosphere*. 2015;9(1):109-121. doi:https://doi.org/10.5194/tc-9-109-2015

61. Hall K. The role of thermal stress fatigue in the breakdown of rock in cold regions. *Geomorphology*. 1999;31(1-4):47-63. doi:10.1016/S0169-555X(99)00072-0

62. Sass O. Rock Moisture Fluctuations During Freeze-thaw Cycles: Preliminary Results from Electrical Resistivity Measurements. *Polar Geogr*. 2004;28(1):13-31. doi:10.1080/789610157

63. Matsuoka N. Direct observation of frost wedging in alpine bedrock. *Earth Surf Process Landf*. 2001;26(6):601-614. doi:10.1002/esp.208

64. McColl ST, Draebing D. Rock Slope Instability in the Proglacial Zone: State of the Art. In: Heckmann T, Morche D, eds. *Geomorphology of Proglacial Systems: Landform and Sediment Dynamics in Recently Deglaciated Alpine Landscapes*. Geography of the Physical Environment. Springer International Publishing; 2019:119-141. doi:10.1007/978-3-319-94184-4_8

65. Matsuoka N, Murton J. Frost weathering: recent advances and future directions. *Permafr Periglac Process*. 2008;19(2):195-210. doi:10.1002/ppp.620

66. Draebing D, Krautblatter M. The Efficacy of Frost Weathering Processes in Alpine Rockwalls. *Geophys Res Lett*. 2019;46(12):6516-6524. doi:10.1029/2019GL081981

67. Jia H, Xiang W, Krautblatter M. Quantifying Rock Fatigue and Decreasing Compressive and Tensile Strength after Repeated Freeze-Thaw Cycles. *Permafr Periglac Process*. 2015;26(4):368-377. doi:10.1002/ppp.1857

68. Vargas EAJr, Veloso RQ, Chavez LE, Gusmão L, Amaral CP. On the Effect of Thermally Induced Stresses in Failures of Some Rock Slopes in Rio de Janeiro, Brazil. *springerprofessional.de*. 2012;46:123-134.

69. Gunzburger Y, Merrien-Soukatchoff V, Guglielmi Y. Influence of daily surface temperature fluctuations on rock slope stability: case study of the Rochers de Valabres slope (France). *Int J Rock Mech Min Sci*. 2005;3(42):331-349. doi:10.1016/j.ijrmms.2004.11.003

70. Robinson PJ. On the Definition of a Heat Wave. *J Appl Meteorol*. 2001;40(4):762-775. doi:10.1175/1520-0450(2001)040<0762:OTDOAH>2.0.CO;2

847 **Table 1.** Summary characteristics of the 209 rockfall events used in this study. MARST refers to the
848 Mean Annual Rock Surface Temperature such as displayed in Figure 1.

	Altitude (m)	**MARST (°C)**	**Volume (m^3)**	**Scar depth (m)**	**Slope angle (°)**
Minimum	2175	-8.7	100	0.8	12*
Mean	3341	-2	1836	3	57
Median	3355	-2	400	3.8	57
Maximum	4085	4	60 000	15	82

849

850 **Table 1:** Optimum parameters for minimizing the RMSE between simulated and real borehole temperatures. * This
851 low value is explained by the fact that the rockfall occurred from the top of a crest.

Parameter	**Value**
Bedrock conductivity ($k_{bedrock}$)	3.3 $W.m^{-1}.K^{-1}$
Bedrock porosity (φ)	1 %
Total water content ($\theta_{w,tot}$)	1 %
Bedrock volumetric heat capacity	2.10^6 $J.m^{-3}.K^{-1}$
Profile resolution	From 1 to 3 m: 0.1 m From 3 to 10 m: 0.2 m From 10 m to 20.5 m: 0.5 m
Spin-up duration	3 years
C_{exp}	4

852